Surface Segregation in SnO_2–Fe_2O_3 Nanopowders and Effects in Mössbauer Spectroscopy

Ricardo H. R. Castro,*[a,b] Pilar Hidalgo,[a] José A. H. Coaquira,[c] Jefferson Bettini,[d] Daniela Zanchet,[d] and Douglas Gouvêa[a]

Keywords: Materials science / Nanostructures / Semiconductors / Electron microscopy / Moessbauer spectroscopy

SnO_2–Fe_2O_3 nanopowders prepared by the polymeric precursor method were studied by combined conventional and high-resolution techniques. The powders treated at 500 °C were analyzed by EDS local probe associated with HRTEM to directly detect surface segregation of Fe ions onto SnO_2 nanoparticles over a broad range of concentrations. The segregation of these ions controls the system microstructure by changing the surface energies and acting as nucleation sites for the formation of a Fe oxide phase (magnetite) at high Fe concentrations. A technologically interesting core–shell-type particle structure, with a magnetic shell and semiconductor core, was observed for the first time. The influence of the segregated Fe ions in Mössbauer spectra is also addressed as a new proposal for the interpretation of the effects of composition changes in both the bulk and at the interface of particles. In this proposal, the two observed sites in Mössbauer spectra would be independently related to bulk-substituted and surface-segregated Fe ions.

Introduction

In the past few decades the electrical and magnetic properties of oxide systems containing Fe ions have greatly increased commercial interest in such materials for application as gas sensors, catalysts and other devices.[1,2] These properties have been extensively studied for many systems,[1–13] and a number of efforts have been carried out to establish the relationship between the observed properties and structural features of these solids. However, since most of the techniques used are not suitable for detecting surface-segregated atoms,[3,9] the discussions rarely consider this phenomenon as a relevant issue, and its influence on the structure and microstructure are usually disregarded. This could lead to incomplete microstructure characterizations that could have reflected in unreliable conclusions about the related properties. In fact, the presence of atoms at the surface can change the interpretation of several phenomena and open up new perspectives for the development of new devices.

Techniques such as X-ray photoelectron spectroscopy (XPS) have shown that surface segregation of components occurs in a wide range of compositions in a large number of systems and, moreover, these segregated components should play an important role in oxide systems.[12–17] This role should involve not only effects on the final properties of the materials, such as electrical and optical, but also on their microstructure and structure evolution.

Although considered an extensive solid-solution system, and with a number of studies concerning this topic,[18–20] surface segregation has recently been hypothesized in the technologically relevant Fe_2O_3–SnO_2 system.[21,22] The hypothesis firstly emerged from the fact that, despite the similarity between the ionic radii of Fe^{3+} and Sn^{4+}, which should induce the formation of an extensive solid solution, Fe_2O_3 (hematite) possesses a corundum-type structure whereas Sn^{4+} hardly forms this structure type and, therefore, their mutual solubility should be lower than that expected by the radius analysis. Actually, only some indirect evidence, fundamentally based on surface IR spectroscopy and surface charges, has indicated that the lower concentration component of this system, instead of forming a bulk solid solution, could be segregating onto the surface of the particles as a surface solid solution. This conclusion was based on the very pronounced effects of the components in the surface sensitivity measurements even at low concentrations and, moreover, on the lack of apparent peak dislocations or second phases in the XRD patterns.[23]

This paper intends to address the surface segregation in the Fe_2O_3–SnO_2 system by using energy dispersive spectroscopy (EDS), XRD, and HRTEM to clarify the ions' distribution in this system and also consider the microstructure of different compositions. Moreover, since the segrega-

[a] Escola Politecnica, Department of Metalurgical and Materials Engineering, University of São Paulo,
Av. Prof. Mello Moraes 2463, São Paulo, SP 05508-900, Brazil
Fax: +55-11-3091-5238
E-mail: ricardo@cecm.usp.br
[b] Centro Universitário da FEI,
Av. Humberto A. C. Branco, 3973, São Bernardo do Campo, SP 09850-901, Brazil
[c] Instituto de Física, University of São Paulo
CP 33618, São Paulo, SP 05315-970, Brazil
[d] Brazilian Synchrotron Light Laboratory, LNLS,
CP 6192, Campinas, SP 13084-971, Brazil

  DOI: 10.1002/ejic.200400879

tion of the lower concentration component on the surface of the power can be confirmed by these techniques, this work also readdresses Mössbauer spectroscopy in this system by taking into account the influence of the segregated components. Although this spectroscopy has been the subject of several studies in this system[3,19] and, moreover, this technique has already been independently described to consist of a crystalline contribution and an interface one,[24] surface segregation and its influence on the interface contribution have not been addressed, and even nowadays, Mössbauer studies of the SnO_2–Fe_2O_3 system are still exclusively based on the same solid-solution concepts.[18]

Results and Discussion

Figure 1(a) shows the XRD patterns of SnO_2 powders containing increasing amounts of Fe prepared by a polymeric precursor method.[25,26] Up to 30 mol-% Fe all reflection peaks can be assigned to the SnO_2 tetragonal phase. In 50 and 80 mol-% Fe samples, additional peaks appear in the XRD patterns indicating a second-phase nucleation that could be related to the (220) and (311) reflections of both

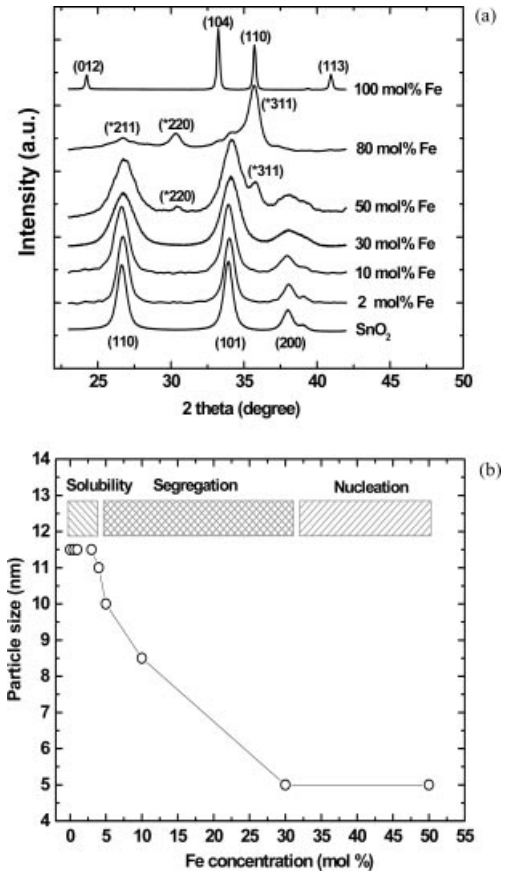

Figure 1. (a) XRD spectra of SnO_2 powders containing different amounts of Fe. The peaks identified by * correspond to the formation of a second phase. (b) SnO_2 particle diameters estimated by the Sherrer method as a function of Fe concentration. Note the three distinct regimes: solubility, segregation, and second-phase nucleation.

magnetite and maghemite phases. The XRD pattern of the 100 mol-% Fe sample corresponds to pure hematite phase.

Since only slight changes can be observed in the diffractograms up to 50 mol-% Fe, one may suggest the solubility and segregation ranges of Fe in the SnO_2 structure to be below 50 mol-% Fe, after which nucleation of the second phase occurs. The solubility range can be determined from the data in Table 1, where the lattice parameters of the SnO_2 phase, extracted from the XRD patterns of 0–10 mol-% Fe samples, are presented. Note that the lattice parameter *a* remains almost constant with increasing Fe concentration, whereas lattice parameter *c* increases with increasing Fe content up to about 4 mol-%. The distortion of the SnO_2 lattice can be attributed to the incorporation of Fe^{3+}, thus suggesting that the solubility limit for this system is around this concentration. A further increase of the Fe content does not significantly change the lattice parameters. Since no crystalline second phases are observed at this stage, both amorphous second phase or the surface segregation of Fe ions can be considered. Based on the literature reports and the HRTEM and EDS data presented below, an amorphous phase can be disregarded. That is to say, after saturation of the lattice by the additive, and above this limit, the segregation of atoms onto the particle surface is supposed to be relatively energetically favorable for the additive. The existence of a solubility limit, however, does not mean that segregation is not occurring before it, but that a smooth transition between both phenomena should exist. This explains why surface-segregation effects are already observed with 2 mol-% Fe but are much more pronounced at about 5 mol-% Fe.[23]

Table 1. Refined values of unit-cell parameters of SnO_2 containing different Fe contents.

Sample	*a* [Å]	*c* [Å]	*c*/*a*
SnO_2[a]	4.7367(1)	3.1855(1)	0.672
SnO_2	4.7406(1)	3.238(4)	0.683
1 mol-% Fe	4.7402(3)	3.263(7)	0.688
2 mol-% Fe	4.7406(2)	3.277(6)	0.691
4 mol-% Fe	4.7401(1)	3.296(7)	0.695
5 mol-% Fe	4.7403(1)	3.291(8)	0.694
10 mol-% Fe	4.7406(5)	3.30(2)	0.696

[a] Data taken from the literature.[27]

The particle size changes as a function of Fe concentration shown in Figure 1(b) reinforce the segregation hypothesis and allow a more precise determination of its occurrence range. The particle diameters were estimated from the XRD peaks by the Sherrer method and confirmed by HRTEM images. Note that below the solubility limit the particle size remains almost constant, suggesting that the inclusion of the additive inside the lattice does not significantly increase the diffusion mechanisms responsible for grain growth. After this point, and between 4 and 30 mol-%, the particle diameters decrease substantially. This is coherent with the proposition of segregation occurrence beyond 4 mol-% Fe, i.e., after the matrix saturation by the additive, an excess of Fe ions segregate onto the particle surfaces, slightly reducing the surface energies and, conse-

quently, decreasing the final particle sizes, as predicted by the Ostwald ripening model.[22,23,28–30] Since the surface energy is highly dependent on the Fe surface concentration, the particle size of the system decreases as the Fe surface concentration increases until the total coverage of the surface, determined as the segregation limit. Above the segregation limit, the nucleation of a second phase becomes energetically favorable for the additive. This is the case for concentrations higher than about 30 mol-%; in this case the SnO_2 particle diameter remains approximately constant.

A local probe technique (EDS) associated with HRTEM images is a conclusive tool to prove surface segregation and is particularly useful for understanding the second-phase nucleation mechanism. Figure 2(a) shows a 2 mol-% Fe micrograph where only SnO_2 particles, identified by the lattice fringes, have been confirmed (corresponding to the (110) planes). Figure 2(b) shows particles of 30 mol-% Fe for comparison. A decrease in particle sizes is clearly seen, as discussed previously.

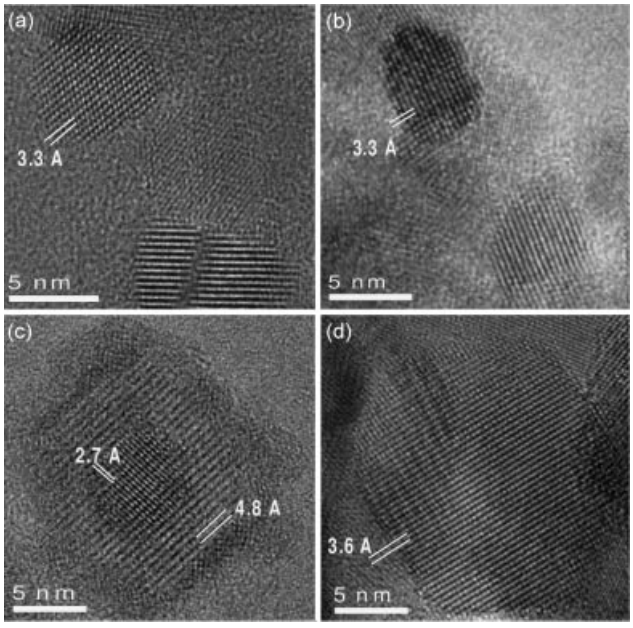

Figure 2. HRTEM images of SnO_2 powders containing: (a) 2, (b) 30, (c) 80, and (d) 100 mol-% Fe. Lattice fringes correspond to (a) and (b) (110) tetragonal SnO_2 planes; (c) core: (101) tetragonal SnO_2 planes, shell: (111) cubic Fe oxide; (d) (110) hematite.

Segregation of Fe onto the surface is, however, only confirmed by EDS measurements when collecting data at the center and at the edge of SnO_2 particles containing different Fe contents (3 nm beam probe). A general EDS was also measured for comparison purposes. Figure 3 compiles the results of the 30 mol-% Fe and demonstrates that there is indeed an excess of Fe ions located on the SnO_2 particle surface. The concentration at the surface is about 1.3-times higher than that computed at the center of this particle. Similar effects are observed in particles containing 10, 50, and 80 mol-% Fe, with different ratios, showing that the segregation occurs in a broad range of compositions. These results are shown in the inset of Figure 3. A relatively high ratio is observed in particles containing 80 mol-% Fe; this is related to the particular second-phase nucleation process, as explained below.

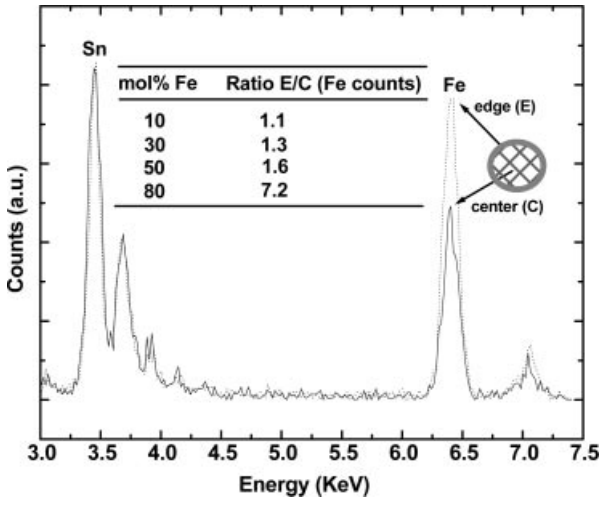

Figure 3. EDS spectra at the center (C) and at the edge (E) of a 30 mol-% Fe particle. Inset: EDS results as a function of Fe concentration, at 6.3 keV. The data is presented as the height peak of the edge-to-center ratio (E/C) after normalization to the Sn peak intensity.

Increasing the Fe content in the SnO_2-based powder saturates the segregation path and induces the second-phase nucleation regime. This was observed by XRD measurements, but the mechanism of the process that takes place and the nature of the new phase could not be conclusively identified. Using HRTEM images both aspects are now better addressed. Figure 2(c) shows an HRTEM image of an 80 mol-% Fe particle, where an interesting core–shell structure can be identified. This result confirms the formation of a second phase and reveals that, in fact, it nucleates on the surface of the SnO_2 particle forming a surface coating. This can be understood based on the segregation of Fe on the surface of SnO_2, where the segregated atoms work as heterogeneous nucleation sites for the new phase growth. Interestingly, since the nucleation occurs on the surface of SnO_2, an epitaxial-type growth may be expected, and a metastable Fe oxide phase other than the thermodynamically stable hematite has been detected. Hematite is the phase formed in the absence of SnO_2 by this synthesis method, as shown by XRD, and confirmed by HRTEM [Figure 2(d); lattice fringes correspond to the (110) planes]. In Figure 2(c), lattice fringes crossing the core–shell structure suggest an epitaxial-type growth. The center of the particle shows the (101) planes of the SnO_2 structure, whereas the shell lattice fringes correspond to either the (111) planar distances of maghemite or magnetite. These results thus explain the high ratio observed for 80 mol-% Fe samples by EDS, indicating that the probe is in fact detecting the Fe_2O_3 surface nucleated phase. The nature of the nucleated phase was further clarified by Mössbauer spectroscopy measurements.

The segregation regime occurring between solid solution and second phase nucleation appears as a new element in this system evolution, and therefore the Mössbauer spectroscopy results should be revised by considering these three additive incorporation regimes. In fact, Mössbauer spectra have already been described to consist of a crystalline component and an interface one.[23] Therefore, especially when dealing with nanometric particle sizes, characterized by a high specific surface area, one may argue that Mössbauer spectroscopy signals may be strongly affected by the segregated atoms, and neglecting this phenomenon may lead to mistaken conclusions.

Figure 4 shows the Mössbauer spectra at room temperature for 2–100 mol-% Fe samples. For 2, 10, and 30 mol-% Fe, the experimental data have been adjusted using least-squares criteria by considering the presence of two doublets (sites I and II). The obtained parameters are shown in Table 2. In this concentration range, only electric quadrupoles (doublets) are detected, with no indication of magnetic hyperfine structures (sextets). A magnetic interaction does not appear even when the data were colleted at 78 K. This indicates that, if there is any superparamagnetic relaxation, it is occurring at temperatures below 78 K. This class of spin relaxation is expected because of the observed small particle sizes (ca. 5 nm) and is related to the relaxation time of the atom spin (spin–spin or spin–orbital) smaller than the Larmor precession time.[31]

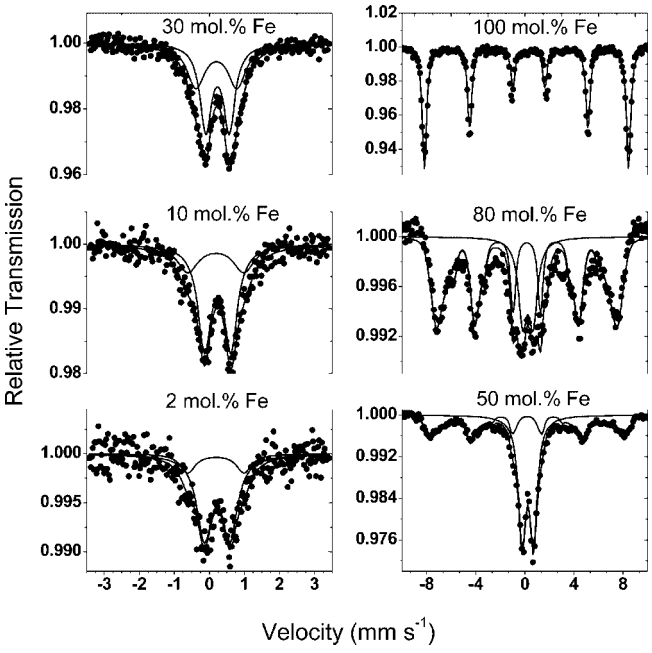

Figure 4. Mössbauer spectra at room temperature for SnO_2 powders containing different contents of Fe.

An important point to note is that the area of site I decreases and that of site II slightly increases with increasing Fe content, as noted in the deconvolution of the peaks. Upon varying the concentration of Fe from 2 to 30 mol-% the area of site I decreases by about 30%. A similar behavior has been observed previously, although no reasonable explanation was given.[19] The phenomenon may be explained by considering the spectra to consist of both interface and bulk contributions. That is to say, each of the observed sites corresponds to a different position of the Fe ions. The Fe atoms located inside the SnO_2 lattice would contribute to the Mössbauer signal in site I and those segregated on the surface would be responsible for the site-II signal. This is coherent with the model described above concerning the solubility and segregation of the low component atom in the system SnO_2–Fe_2O_3. Since the solubility limit is observed at about 4 mol-% for the Fe ion in the SnO_2 lattice, any further increase in the concentration of the additive causes it to segregate on the surface. Such segregated atoms are not well crystallized and give rise to high electric quadrupoles due to local lattice distortions. With increasing Fe content, the surface coating is increased, and the site-II area increases as well.

Such an area increase in the Mössbauer spectra is observed until the second-phase nucleation occurs. Therefore, a nuclear hyperfine magnetic structure is observed for the powder containing 50 mol-% of Fe_2O_3. This hyperfine magnetic structure is the same as that detected in the 80 mol-% Fe_2O_3 sample, but different from that observed for 100 mol-% Fe (hematite). Since the hyperfine parameters of maghemite and magnetite are very similar,[31,32] these data confirm the presence of the new phase but could not be used to clearly identify the phase. Note the presence of the doublet due to Fe ions incorporated in the SnO_2 lattice (site I) when dealing with the samples with 50 and 80 mol-% Fe, which is related to the SnO_2 cores found by the micrograph [Figure 2(c)] saturated by Fe ions. Site II, related to segregated Fe, is not observed in these samples since it has been replaced by the hyperfine magnetic structure grown on the surface.

Table 2. Mössbauer spectroscopy parameters. Isomer shifts are related to metallic Fe. 50 and 80 mol-% samples were fitted with just one doublet and a magnetic sextet; 100 mol-% sample has just the magnetic component as presented in the table. HF means hyperfine field in Tesla [T]. Site I is related to Fe inside SnO_2 lattice. Site II is related to surface-segregated Fe.

	Site I			Site II			Magnetic site			
Fe [mol%]	QS [mm s^{-1}]	IS [mm s^{-1}]	AE [%]	QS [mm s^{-1}]	IS [mm s^{-1}]	AE [%]	QS [mm s^{-1}]	IS [mm s^{-1}]	HF [T]	AE [%]
2	0.731(40)	0.306(10)	81(5)	1.60(17)	0.270(50)	19(5)	–	–	–	–
10	0.751(18)	0.323(6)	70(4)	1.60(12	0.268(26)	30(4)	–	–	–	–
30	0.672(19)	0.317(4)	56(5)	1.17(9)	0.285(10)	44(5)	–	–	–	–
50	0.930(6)	0.351(3)	58(5)	–	–	–	0.012(22)	0.303(12)	43.6(2)	42(5)
80	0.847(29)	0.357(9)	28(5)	–	–	–	0.008(14)	0.267(10)	43.6(2)	72(5)
100	–	–	–	–	–	–	0.194(4)	0.341(2)	51.5(2)	100

Conclusions

The distribution of the components in SnO_2–Fe_2O_3 nanopowders in different compositions can be understood based on the correlation of XRD with spatial high-resolution characterization tools, such as EDS and HRTEM, thus avoiding the loss of information about segregated components. At lower concentration (<4 mol-%), the Fe ions are preferentially incorporated in the SnO_2 lattice to form a solid solution; at intermediate values (4–30 mol-%) the Fe ions segregate onto the SnO_2 surface, as confirmed by EDS. The segregated atoms have important effects in Mössbauer spectroscopy measurements, suggesting that the spectra are a combination of the independent effects of bulk and interface components. At higher concentrations (>30 mol-%) a second phase is nucleated and corresponds to an unexpected magnetite or maghemite phase. Core–shell-type particles with an SnO_2 core structure and a magnetic shell structure are observed for the first time at high Fe contents.

Experimental Section

SnO_2–Fe_2O_3 nanopowders were prepared based on Pechini's method.[24] The process can be briefly described as follows: (a) The cationic precursors were introduced into a mixture of ethylene glycol (20.6 wt.-%) and citric acid (47.7 wt.-%). $Sn_2(C_6O_7H_4)\cdot H_2O$ (tin citrate, prepared from $SnCl_2\cdot 2H_2O$; Synth P.A.) and $Fe(NO_3)_3\cdot 9H_2O$ (Synth P.A.) were used as the precursors and HNO_3 was added to the system to promote the solubilization of the citrate. The amounts of precursors were calculated to achieve the desired molar concentrations. (b) The prepared solution was heated to 180–200 °C to promote polyesterification, i.e. polymerization between citric acid and ethylene glycol to give rise to a polymer chain with sites available to react with the ions present. These sites randomly react with tin or iron ions. (c) The obtained liquid precursor was thermally treated at 450 °C for 4 h to give a dry carbon-rich powder. After grinding, the powder was treated at 500 °C for 15 h to guarantee total carbon elimination and an energetically stable distribution of the additives and particle size.[22,25,26] XRD measurements were carried out with a Philips X'Pert MPD diffractometer, using Cu-K_α radiation (λ = 1.5406 Å), at room temperature. A step of 0.05° with an exposure time of 5 s per step was used in the measurements. To determine the lattice parameters, however, XRD was carried out using θ = 0.02° with an exposure time of 10 s and using an internal Si standard. Mössbauer spectra were obtained in the transmission geometry and the γ-radiation source was ^{57}Co atoms immersed in an Rh matrix. The radioactive source was mounted in a constant acceleration transductor and the maximum speed was determined by calibrating the system with a metallic Fe sheet; γ-ray detection was carried out with a proportional detector and the electronically amplified signal was sent to a digital analyzer. EDS and HRTEM images were acquired with a JEM 3010 URP microscope operating at 300 keV (0.17 nm resolution). For EDS a 3-nm beam-size was used and the background obtained for the Cu grid was then subtracted.

Acknowledgments

The authors thank CAPES (Coordenação do Aperfeiçoamento de Pessoal de Nível Superior) and FAPESP (Fundação de Amparo à Pesquisa do Estado de São Paulo) processes 96/09604-9, 99/10798-0, and 01/10053-7 for financial support. LME/LNLS is acknowledged for the use of HRTEM. LSI/EPUSP is acknowledged for help with the electrical measurements.

[1] P. Poizot, S. Laruelle, S. Grugeon, L. Dupont, J. M. Tarascon, *Nature* **2000**, *407*, 496–499.
[2] T. Matsumura, N. Sonouama, R. Kanno, M. Takano, *Solid State Ionics* **2003**, *158*, 253–260.
[3] S. Ichiba, T. Yamaguchi, *Chem. Lett.* **1984**, *10*, 1681–1682.
[4] S. Popovic, B. Grzeta, G. Stefanic, I. CzakoNagy, S. J. Music, *J. Alloys Compd.* **1996**, *241*, 10–15.
[5] M. Ristic, S. Popovic, M. Tonkovic, S. J. Music, *J. Macromol. Sci., Chem.* **2000**, *407*, 496.
[6] P. Polzot, *Nature* **2000**, *407*, 496.
[7] G. Stefanic, S. J. Music, S. Popovic, K. Nomura, *J. Mol. Struct.* **1999**, *481*, 627–631.
[8] M. Ristic, I. Nowik, S. Popovic, S. Music, *Croat. Chem. Acta* **2000**, *73*, 525–540.
[9] F. Schneider, K. Melzer, H. Mehner, G. Dehe, *Phys. Status Solidi A* **1977**, *39*, K115–K117.
[10] V. G. Bhide, S. K. Data, *J. Inorg. Nucl. Chem.* **1969**, *31*, 2394.
[11] M. Takano, *J. Solid State Chem.* **1987**, *68*, 153–162.
[12] D. A. Hramov, V. S. Urusivm, *Akad. Izv. Nauk. SSSR Neorg. Mater.* **1983**, *11*, 1880.
[13] F. Berthier, J. Creuze, R. Tetot, B. Legrand, *Phys. Rev. B: Condens. Matter* **2002**, *65*, 195413.
[14] A. V. Ruban, H. L. Skriver, J. K. Norskov, *Phys. Rev. B: Condens. Matter* **1999**, *59*, 15990–16000.
[15] D. Szczuko, J. Werner, S. Oswald, G. Behr, K. Wetzig, *Appl. Surf. Sci.* **2001**, *179*, 301–306.
[16] G. Bozzolo, J. Ferrante, R. D. Noebe, B. Good, F. S. Honecy, P. Abel, *Comp. Mater. Sci.* **1999**, *15*, 169–195.
[17] B. Slater, C. R. A. Catlow, D. H. Gay, D. E. Williams, V. Dusastre, *J. Phys. Chem. B* **1999**, *103*, 10644–10650.
[18] H. Dulli, P. A. Dowben, S. H. Liou, E. W. Plummer, *Phys. Rev. B: Condens. Matter.* **2000**, *62*, 14629–14632.
[19] M. Sorescua, L. Diamandescua, D. Tarabasanu-Mihailab, V. S. Teodorescub, B. H. Howard, *J. Phys. Chem. Solids* **2004**, *65*, 1021–1029.
[20] S. J. Music, S. Popovic, M. Metikoshukovic, V. Gvozdic, *J. Mater. Sci. Lett.* **1991**, *10*, 197–200.
[21] R. Ruck, Y. Dusausoy, C. N. Trung, J. M. Gaite, A. Murciego, *Eur. J. Mineral.* **1989**, *1*, 343–352.
[22] R. H. R. Castro, P. Hidalgo, P. Hidalgo, R. Muccillo, D. Gouvea, *Appl. Surf. Sci.* **2003**, *214*, 172–177.
[23] G. J. Pereira, R. H. R. Castro, D. Gouvea, *Appl. Surf. Sci.* **2002**, *195*, 274–280.
[24] C. H. Shek, G. M. Lin, J. K. L. Lai, *Nanostruct. Mater.* **1999**, *11*, 831–835.
[25] M. Pechini, US patent no. 3330697, **1967**.
[26] D. Gouvea, R. L. Villalobos, J. D. T. Capocchi, *Mater. Sci. Forum* **1999**, *299*, 91–96.
[27] J. Haines, J. M. Léger, *Phys. Rev. B* **1997**, *55*, 11144.
[28] D. Gouvea, J. A. Varela, E. Longo, A. Smith, J. P. Bonnet, *Eur. J. Solid State Inorg. Chem.* **1993**, *30*, 915.
[29] S. H. Overbury, P. A. Bertrand, G. A. Somorjai, *Chem. Rev.* **1975**, *75*, 547–560.
[30] Y.-M. Chiang, D. Birnie, W. D. Kingery, *Physical Ceramics – Principles for Ceramic Science and Engineering*, John Wiley & Sons Inc., New York, **1997**.
[31] V. I. Goldanskii, E. F. Makarov, *Chemical Applications of Mössbauer Spectroscopy*, Academic Press, New York, **1968**.
[32] Q. A. Pankhurst, R. J. Pollard, in *Mössbauer Spectroscopy Applied to Magnetism and Materials Science* (Eds.: J. Long, F. Granjean), Plenum Press, New York, **1993**, vol. 1.

Received: October 19, 2004